Renewable Energy 128 (2018) 163–176

Contents lists available at ScienceDirect

Renewable Energy

journal homepage: www.elsevier.com/locate/renene

Wave forecast and its application to the optimal control of offshore floating wind turbine for load mitigation

Yu Ma [a, *], Paul D. Sclavounos [a], John Cross-Whiter [b], Dhiraj Arora [c]

[a] Department of Mechanical Engineering, Massachusetts Institute of Technology, Cambridge, MA 02139, USA
[b] Glosten Associates, Seattle, WA 98101, USA
[c] GE Renewable Energy, Richmond, VA 23237, USA

ARTICLE INFO

Article history:
Received 2 February 2018
Received in revised form
26 April 2018
Accepted 16 May 2018
Available online 21 May 2018

Keywords:
Offshore floating wind turbine
Wave forecast
Optimal control
Load reduction

ABSTRACT

Control algorithms play an important role in energy capture and load mitigation for offshore floating wind turbines (OFWTs). One of the advanced and effective control techniques is the feedforward or model predictive control approach, which requires the forecast of incoming environment conditions. For OFWTs, wave loading is one of the dominant sources to excite structural responses. This study is thus motivated to develop forecasting algorithms for wave elevations and wave excitation forces with the purpose of applying feedforward controllers on OFWTs. Two forecasting algorithms, the approximate Prony Method based on ESPRIT (Estimation of Signal Parameters via Rotational Invariance Techniques) and SVM (Support Vector Machine) regression, are developed and validated using wave records from tank tests. Utilizing the forecasted wave elevations and wave excitation forces, a feedforward LQR controller is designed to mitigate structural loads of an OFWT system.

1. Introduction

The ocean environment provides enormous sources of renewable energy, among which one of the most promising is the offshore wind energy. A recent trend of the wind industry is to go further offshore to overcome limited land availability and avoid visual and acoustic pollution. Besides, the ocean wind tends to blow more strongly and consistently, allowing the utilization of larger wind turbines that enjoy better economics per rated megawatt (MW). Meanwhile, using floating support structures in offshore wind farms adds more complexity to the system and leads to more technical and economic challenges. One important aspect of current research aiming to overcome such challenges is to develop advanced control systems to optimize energy capture or achieve load mitigation.

Several advanced control approaches were proposed over the last decades to achieve load reduction or power optimization of onshore and offshore wind turbines. One promising approach is to use feedforward or model predictive control (MPC) to improve disturbance rejection. Extensive studies have been done on model predictive controls on onshore and offshore wind turbines with regard to wind induced loading [1]; [2]; [3]. These studies have shown that, with a model predictive controller, the fatigue loads at critical structural sections can be significantly reduced when wind speed predictions are provided to the controller.

So far, the majority of studies on advanced control algorithms target the mitigation of loads induced by incoming wind speed. For offshore floating wind turbines, wave excitation force is also a dominant persistent disturbance that excites dynamic and structural responses. Control issues for modeling floating wind turbines were studied earlier with regard to the coupling between the pitch controller and the platform motion [4]; [5]. Without adjustment, such coupling effects would cause negatively damped responses thus resulting in instability of the system. However, little research has been done aiming at load reduction by resisting wave disturbance via similar advanced control approaches.

Furthermore, an implementation of such optimal control designed to resist wave disturbance requires a sufficiently accurate prediction of wave elevations or wave excitation forces in the time domain. Efforts have been made to predict wave elevations or wave excitation forces by various approaches. Hals et al. [6] used the augmented Kalman filter with a simple damped harmonic oscillator to model and predict the wave forces with a forecast horizon 2.2 s under an irregular sea state for their model predictive

* Corresponding author.
E-mail address: yuma@mit.edu (Y. Ma).

https://doi.org/10.1016/j.renene.2018.05.059
0960-1481/

controller. Fusco & Ringwood [7] compared four different approaches for predicting short-term wave elevations, which were cyclical models, sinusoidal extrapolation with the Extended Kalman filter, autoregressive models, and neutral networks. The prediction models were validated using field measurements from two sites. Casanovas [8] compared the performance of autoregressive models and ESPRIT (Estimation of Signal Parameters via Rotational Invariance Techniques) models to forecast wave elevations. Although some work has been done on this issue, there are still gaps to achieve real-time implementation. Hals et al. [6] stated that the forecast horizon and accuracy had a great impact on the overall performance of the MPC algorithm. The augmented Kalman filter did not fulfil such requirements very well even though it was tested by simulated sea states. Fusco & Ringwood [7] used ideal non-causal filters to preprocess the raw wave elevations to get a better forecast performance, which could not be implemented in real-time. Casanovas [8] validated the AR and ESPRIT model using simulated wave elevations, which contained no noise thus much easier to predict.

Therefore, more refined methods to predict real-time wave elevations and wave excitation forces need to be developed and validated. Also, the performance of optimal control algorithms for offshore floating wind turbines need to be validated under real-time prediction of wave elevations or wave excitation forces instead of an assumption of perfect prediction.

The present paper applies a predictive model based LQR controller to minimize the structural loads of a floating wind turbine. To achieve such an optimal controller, the prediction of wave elevations or wave excitation forces needs to be provided. Two approaches, the approximate Prony method based on ESPRIT and the SVM (Support Vector Machines) regression, are proposed to forecast short-term wave elevations and wave excitation forces. The predictors and controllers are integrated and validated against a TLP (Tension Leg Platform) type floating wind turbine. Measured wave records from tank tests are used to validate the forecast algorithms. The performance of the optimal control algorithm is compared with a baseline Proportional-Integral (PI) controller.

2. Short-term forecast algorithms

2.1. Approximate Prony Method based on ESPRIT

The approximate Prony method based on ESPRIT [9] is a method that identifies signals composed of complex exponentials, which is essentially based on the Singular Value Decomposition (SVD) of a specially constructed Hankel matrix. This signal processing technique has been widely used in speech enhancement and recognition, direction of arrival estimation of sensor arrays, time series analysis and forecasting, etc.

In principle, the Prony-type method or polynomial methods identify the exponents from the roots of a characteristic polynomial. The variants of this method differ in the way the coefficients of the polynomial are defined, which would extend the Prony method for extracting exponential signals from uniformly sampled time series data when there is no noise to the case when the signal is embedded in noise. The algorithm introduced in this study uses a truncated singular value decomposition of a Hankel matrix defined by the noisy signal to solve for the polynomial coefficients, which allows one to determine the number of representative exponential terms of the signal that is appropriate for the noise level [10].

Consider a sampled signal h_k which can be expressed as:

$$h_k = \sum_{j=1}^{M} \rho_j z_j^k, k = 1, 2, ..., N \tag{1}$$

where, N is the number of samples.

M is the order of the exponentials, which is unknown.

Based on the theory of Prony-like methods, z_j are eigenvalues of the matrix pencil:

$$zH_{N-L,L}(0) - H_{N-L,L}(1) \tag{2}$$

where, the Hankel matrix H is $H_{N-L,L}(s) := (h(s+r+m))_{m,r=0}^{N-L-1,L-1}(s = 0, 1)$.

$L \geq M$ is a parameter representing the upper bound of the exponential order M.

To solve the eigenvalue problem described in (2), the algorithm is formed as follows:

a. Form the rectangular Hankel matrix:

$$H := (h_{k+l})_{k,l=0}^{N-L-1,L} \tag{3}$$

b. Carry out a singular value decomposition of H:

$$H = U\Sigma V^* \tag{4}$$

c. Form the matrices:

$$V_1 := V(1 : L, 1 : L) \tag{5}$$

$$V_2 := V(2 : L + 1, 1 : L) \tag{6}$$

$$F := V_1^+ V_2 \tag{7}$$

where, $V_1^+ := (V_1^* V_1)^{-1} V_1^*$ is the Moore-Penrose pseudoinverse of V_1.

d. Compute the eigenvalues z_j , j = 1,2, …,L, of the matrix F

e. Compute ρ_j as the least squares solution of the overdetermined linear Vandermonde-type system:

$$h_k = \sum_{j=1}^{L} \rho_j z_j^k, k = 1, 2, ..., N \tag{8}$$

f. Set a tolerance bound ε, delete all the pairs (z_j, ρ_j) with $|\rho_j| \leq \varepsilon$ and denote the remaining exponential set by $\{z_j : j = 1, ..., M\}$ with $M \leq L$.

g. Repeat step e and solve the new overdetermined linear Vandermonde-type system with order M again:

$$h_k = \sum_{j=1}^{M} \rho_j z_j^k, k = 1, 2, ..., N \tag{9}$$

Output: $\rho_j, z_j, j = 1, ..., M$.

Based on linear wave theory, measured or simulated wave elevations in unidirectional seas can be decomposed as:

$$\eta(t) = \sum_{j=-\infty}^{\infty} A_j e^{i\omega_j t + i\phi_j} + e_j \tag{10}$$

where, $\eta(t)$ is the real-time wave elevations and e_j is the noise. ω_j is

the jth wave frequency, A_j and ϕ_j are the corresponding amplitude and phase.

Clearly, the simulated or measured wave elevation with a sampling rate Δt can be expressed in a form similar to (1):

$$\eta_k = \sum_{j=1}^{M} \rho_j z_j^k \tag{11}$$

where, η_k is the sampled wave record, k = 1,2 …,N.

The complex amplitudes $A_j e^{i\phi_j}$ are represented by ρ_j.

The complex exponentials $e^{i\omega_j t}$ are represented by z_j^k by converting $t = k\Delta t, z_j = e^{i\omega_j \Delta t}$.

Using the algorithm described by Eq. (3)-Eq. (9), the wave records over a certain length of time can be fitted by complex frequencies and amplitudes (ρ_j, z_j). Correspondingly, the forecasted wave elevations can be expressed as:

$$\eta_k = \sum_{j=1}^{M} \rho_j z_j^k, k = N+1, \ldots, N+N_{forecast} \tag{12}$$

where, $N_{forecast}$ is the forecast horizon.

Similarly, under linear wave potential theory, the wave excitation forces can be expressed using exactly the same form (Eq. (13)) with that of wave elevations (Eq. (10)) and thus can be forecasted in the same way as Eqs. (3)–(9) and (12).

$$F_e(t) = \sum_{j=-\infty}^{\infty} F_j e^{i\omega_j t + i\psi_j} + \varepsilon_j \tag{13}$$

where, $F_e(t)$ is the real-time wave excitation forces. ε_j is the noise contained in the simulation or measurements. ω_j is the jth wave frequency, F_j and ψ_j are the corresponding amplitude and phase.

2.2. Least-squares Support Vector Machines (LS-SVM) regression

SVM regression is a powerful machine learning method which has been successfully used for time-series prediction in various fields [11]; [12]; [13]. It uses a hypothesis space of linear functions in a high dimensional feature space, which is trained with a learning algorithm from optimization theory that implements a learning bias derived from statistical learning theory. LS-SVM [14] is the least-squares version of standard SVM, which solves a set of linear equations instead of a convex quadratic programming (QP) problem of classical SVM.

The general SVM regression model estimates the forecasted signal from a high dimensional feature space of the input vector:

$$y_f = w^T \phi(\mathbf{x}) + b \tag{14}$$

where, y_f is the signal to be forecasted. $\mathbf{x}$ is the input vector of features, $\mathbf{x} = (x^1, x^2, \ldots x^k)^T$. w is the weight vector. $\phi(\cdot)$ is the feature mapping function. b is the bias term.

Given a sample of training data $\{(\mathbf{x_i}, y_i)\}_{i=1}^{N}$, LS-SVM determines the optimal weight vector and bias term by minimizing the cost function R:

$$\min_{w,e} R(w,e) = \frac{1}{2}\|w\|^2 + \frac{1}{2}\gamma\|e\|^2 \tag{15}$$

subject to the equality constraints:

$$y_i = w^T \phi(\mathbf{x_i}) + b + e_i, i = 1, 2, \ldots, N \tag{16}$$

where, $\|\cdot\|$ denotes the Euclidean norm. γ is the regularization parameter which controls the trade-off between the bias and variance of LS-SVM model. $\mathbf{e}$ is the error vector, $\mathbf{e} = (e_1, e_2, \ldots, e_N)^T$.

Eqs. (15)-(16) form a standard optimization problem with equality constraints. The Lagrangian of such a problem is:

$$L(w,b,e,\lambda) = R(w,e) - \sum_{i=1}^{N} \lambda_i \left(w^T \phi(\mathbf{x_i}) + b + e_i - y_i \right) \tag{17}$$

where, λ_i are the Lagrange multipliers.

According to the Karush-Kuhn-Tucker Theorem, the conditions of optimality are:

$$\begin{aligned} &\frac{\partial L}{\partial w} = 0 \rightarrow w = \sum_{i=1}^{N} \lambda_i \phi(\mathbf{x_i}) \\ &\frac{\partial L}{\partial b} = 0 \rightarrow \sum_{i=1}^{N} \lambda_i = 0 \\ &\frac{\partial L}{\partial e_i} = 0 \rightarrow \lambda_i = \gamma e_i \\ &\frac{\partial L}{\partial \lambda_i} = 0 \rightarrow w^T \phi(\mathbf{x_i}) + b + e_i - y_i = 0 \end{aligned} \tag{18}$$

Cast Eq. (18) into a linear matrix equation:

$$\begin{bmatrix} 0 & \vec{1}^{\mathbf{T}} \\ \vec{1} & \mathbf{K} + \gamma^{-1}\mathbf{I} \end{bmatrix} \begin{bmatrix} b \\ \lambda \end{bmatrix} = \begin{bmatrix} 0 \\ \mathbf{y} \end{bmatrix} \tag{19}$$

where, $\vec{1} = (1, 1, \ldots, 1)^T$. $\mathbf{I}$ is the identity matrix. $\mathbf{y} = (y_1, y_2, \ldots y_N)^T$. $\mathbf{K} = (k(\mathbf{x_i}, \mathbf{x_j}))_{i,j=1}^{N}$ is called the kernel matrix, and $k(\mathbf{x_i}, \mathbf{x_j}) = \phi^T(\mathbf{x_i})\phi(\mathbf{x_j})$.

Then, the forecasted signal using the LS-SVM regression model can be expressed as:

$$y_f = \sum_{i=1}^{N} \lambda_i k(\mathbf{x}, \mathbf{x}_i) + b \tag{20}$$

From Eqs. (19)-(20), it can be seen that the mapping function $\phi(\mathbf{x})$ does not need to be known explicitly. All LS-SVM requires is the inner product of $\phi(\mathbf{x})$, i.e., the kernel function $k(\mathbf{x_i}, \mathbf{x_j})$. Some widely used kernel functions take the form of linear, polynomial and Gaussian functions. In this study, the popular Gaussian kernel is used:

$$k(\mathbf{x}, z) = \exp\left(-\|\mathbf{x} - z\|^2 \Big/ \sigma^2 \right) \tag{21}$$

where, $\|\cdot\|$ denotes the 2-norm of a vector. σ is a constant determining the width of the Gaussian kernel.

Eqs. (14)-(21) above describes the general principle of LS-SVM regression method. To implement LS-SVM regression to achieve the prediction of wave elevations or wave excitation forces, consider a one-step ahead prediction for a time series using the autoregressive model first:

$$\eta_{t+1} = f(\eta_t, \eta_{t-1}, \ldots, \eta_{t-d+1}) \tag{22}$$

where, η_t denotes the sampled time series. d is the order of autoregressive model.

In the context of the LS-SVM, the training data $\{\mathbf{x_i}, y_i\}_{i=1}^{N_{training}}$ would be formatted as:

$$\begin{aligned} \mathbf{x_i} &= \left[\eta_{t_i}, \eta_{t_i-1}, \ldots, \eta_{t_i-d+1}\right] \\ y_i &= \eta_{t_i+1} \end{aligned} \tag{23}$$

where, $N_{training}$ is the number of the data sets used in the training procedure.

After training, Eq. (19) is solved. Denote the current time as t_c, then for one-step ahead prediction, the input and output in Eq. (20)

is:

$$\begin{aligned}\mathbf{x} &= \left[\eta_{t_c}, \eta_{t_c-1}, \ldots, \eta_{t_c-d+1}\right] \\ y_f &= \eta_{t_c+1}\end{aligned} \tag{24}$$

To achieve multi-step ahead prediction, one only needs to repeat the one-step ahead prediction multiple times, substituting the output y_i in Eq. (23) as η_{t_i+k} in the training step and similarly y_f in Eq. (24) as η_{t_c+k} in the forecast (k = 1,2, …, $N_{forecast}$).

3. The optimal control formulation

The offshore floating wind turbines are compliant to both wind and wave induced loads. The baseline controller of the wind turbine system at above rated wind speed is mainly designed to regulate the rotor speed to reduce power fluctuation using a PI control. In this study, an overlaid optimal control is proposed aiming to additionally mitigate the fore-aft tower base bending moment, which is largely excited by ocean waves. For both the baseline and overlaid optimal control designs, the approach of collective blade pitch control is used. To achieve such an objective, the wave excitation forces are modelled as persistent external disturbances that need to be evaluated and forecasted.

The linearized system dynamics around an operation point can be represented as a state space model:

$$\begin{aligned}\dot{x}(t) &= Ax(t) + Bu(t) + f_e(t) \\ y(t) &= Cx(t) + Du(t)\end{aligned} \tag{25}$$

A, B, C, D are the associated state, input and output matrices.

The objective is to find an optimal control law u_{opt} such that:

$$\begin{aligned}u_{opt}(t) &= \underset{u}{\operatorname{argmin}} J(u) \\ &= \frac{1}{2}\int_{t_0}^{t_0+T}\left(x^TQx + u^TRu + 2u^TSx\right)dt \\ &\quad + \frac{1}{2}x(t_0+T)^TGx(t_0+T)\end{aligned} \tag{26}$$

where, t_0 is the present time. T is the optimization horizon. Q, R, S, G are the weighting matrices penalizing the states, control efforts, cross term of states and control efforts and the final time states, respectively.

Thus, the optimization problem is to find an optimal solution of (26) subject to the linear constraints (25). The optimal control law u_{opt} under such a problem takes a generalized state feedback form [15]:

$$u_{opt} = -R^{-1}\left[\left(B^TP(t) + S\right)\bar{x}(t) + B^T\phi(t)\right], t \in [t_0, t_0+T] \tag{27}$$

$$\begin{cases}\dot{P}(t) = P(t)BR^{-1}B^TP(t) - Q + S^TR^{-1}S - P(t)\left(A - BR^{-1}S\right) - \left(A - BR^{-1}S\right)^TP(t) \\ P(t_0+T) = G\end{cases} \tag{28}$$

$P(t), \phi(t), \bar{x}(t)$ are solutions of the following ODEs (ordinary differential equations):

$$\begin{cases}\dot{\phi}(t) = \left[P(t)BR^{-1}B^T - \left(A - BR^{-1}S\right)^T\right]\phi(t) - P(t)f_e(t), t \in [t_0, t_0+T] \\ \phi(t_0+T) = 0\end{cases} \tag{29}$$

$$\begin{cases}\dot{\bar{x}}(t) = \left\{A - BR^{-1}\left[B^TP(t) + S\right]\right\}\bar{x}(t) - BR^{-1}B^T\phi(t) + f_e(t), t \in [t_0, t_0+T] \\ \bar{x}(t_0) = x(t_0)\end{cases} \tag{30}$$

where, $f_e(t)$ represents the external disturbance, i.e. wave induced loads in this study.

$x(t), u(t), y(t)$ are the system states, input and output perturbations around an operation point.

The ODEs (28) and (29) have a known final value and thus need to be solved backwards in time. Making a change of variable $t' = t_0 + T - t$, Eqs. (28)-(29) can be transformed into initial value problems as:

$$\begin{cases}\dot{P}(t') = -P(t_0+T-t')BR^{-1}B^TP(t_0+T-t') + Q - S^TR^{-1}S + P(t_0+T-t')\left(A - BR^{-1}S\right) \\ + \left(A - BR^{-1}S\right)^TP(t_0+T-t'),\ t' \in [0, T] \\ P(0) = G\end{cases} \tag{31}$$

$$\begin{cases} \dot{\phi}(t') = -\left[P(t_0+T-t')BR^{-1}B^T - \left(A - BR^{-1}S\right)^T\right]\phi(t_0+T-t') + P(t_0+T-t')f_e(t_0+T-t'), \\ t' \in [0,T] \\ \phi(0) = 0 \end{cases} \tag{32}$$

Eqs. (30)-(32) are initial value ODE problems, which can be solved by numerical methods such as ABM4 (Adams-Bashforth-Moulton 4th order predictor-corrector) method. Once the optimal control law u_{opt} is solved, the system dynamics would be updated as:

$$\begin{aligned} \dot{x}(t) &= Ax(t) + Bu_{opt}(t) + f_e(t) \\ y(t) &= Cx(t) + Du_{opt}(t) \end{aligned} \tag{33}$$

4. Validation of forecast algorithms

In this application of the optimal control of offshore floating wind turbines, the physical quantity that needs to be evaluated and forecasted is the wave excitation force. In real-time implementation, two approaches may be used to obtain the wave excitation force. One is to use real-time wave elevation measurements such as on-board wave probes or remote wave sensing techniques [16]. Then the wave loads can be simulated by priori derived frequency domain transfer functions. Such transfer functions can be computed using penal method codes based on linear and second-order wave potential theory such as WAMIT [17]. Another approach is to use on-board measurements of motion and structural responses to inversely evaluate the wave excitation forces based on pre-simulated system dynamics. Either way, the derivation of wave excitation forces would contain noise terms due to inaccurate measurements or modeling errors.

Ideally, due to the physical essence of wave excitation forces and platform motions, the floating structure itself can be treated as a natural low-pass filter. Therefore, the wave excitation forces contain lower frequency components and less noise than ambient wave elevations. Taking account of the additional noise due to inaccurate measurements or modeling errors, as stated in (10) and (13), the time series of wave elevation records and wave excitation forces essentially have the same characteristics. Therefore, to better validate the forecast algorithms under real-world noise, records of wave elevations measured in tank tests are considered as a good representation of real-time input signal for the evaluation of wave excitation forces. The two forecast algorithms, approximate Prony method based on ESPRIT and LS-SVM regression method, are implemented and compared.

For the approximate Prony method based on ESPRIT described in (2)–(9), there are three parameters affecting the accuracy of the forecast. One parameter is the number of the training samples N, one is the upper bound of the number of the complex exponentials L and one is the bound ε to determine the actual number of complex exponentials eliminating the components regarded as noise. The choice of these three parameters can be specified for each record since the noise level and dominant frequency components can vary as time marches for different sea states. In this study, we have done multiple sensitivity studies to get the most consistent and robust results as time marching for one wave record as well as for multiple wave records using fixed parameters. Based on these sensitivity studies, reasonable values for ε are $e^{-8} \sim e^{-10}$. The number of training samples N in time scale are in the range of 3–6 wave typical periods, and the upper bound of frequency terms L needs to be set close to N (approximately N-10).

For the LS-SVM regression method, there are two parameters in the training process that need to be specified based on the characteristics of the signal, namely the order of the autoregressive model d in (22) and the number of training samples $N_{training}$ in (23). Besides, there are two hyperparameters of the model itself, the regulation parameter γ in (15) and the kernel width parameter σ in (21), that needs to be optimized. Similar to the approximate Prony method based on ESPRIT, the order of the autoregressive model d and the number of training samples $N_{training}$ are determined based on sensitivity studies to get the most consistent and robust results as well. The order of the autoregressive model is around 1–2 typical wave periods and the number of training samples in time scale is about 50–60 typical wave periods. The two hyperparameters are tuned automatically using 10-fold cross-validation (K. [18] for each forecast.

Two different sea states are tested to validate and compare the two forecast algorithms. One is a mild operational sea state with significant wave height (Hs) 1.7 m and typical wave period (Tp) 8.7 s, while the other one is a more severe sea state with Hs 4.5 m and Tp 11.8 s.

The measured wave records are 2.5-h long. The sampling rate of the original tank wave records is 0.0707 s, and resampled with sampling rate 0.495 s. The forecast horizon is 5 s. Three 300-s segments are tested here as examples to show the performance of the algorithm, which are located at 6000s–6300s, 9000s–9300s and 11000–11300s of the records.

The RMS error of the forecasted signal is defined as:

$$RMS\ error = \sqrt{\frac{1}{N}\sum_{k=1}^{N}\left|\tilde{\eta}_k - \eta_k\right|^2} \tag{34}$$

where, $\tilde{\eta}_k$ is the forecasted wave elevation. η_k is the original wave elevation. To better evaluate the forecast performance, the RMS error is normalized using the significant wave height Hs.

The statistical results of the forecast error and algorithm parameters are listed in Table 1. The overall RMS error of the entire forecasted signal of the three segments is summarized. Besides, the maximum RMS error occurred of each 5-s forecast horizon is listed as a measure of worst-case performance. The number of training samples used in the two methods as well as the order of the autoregressive model for LS-SVM regression are listed here as a measure of the computational cost. Comparisons of the original and forecasted wave elevations of one segment are shown here to give a sketch of the forecast performance (Figs. 1 and 2).

All the tested records above are the original measured wave records without any filtering. As mentioned before, the real-time measured wave elevations contain unknown noise. To forecast a time series, a challenge is to learn higher frequency components of the signal itself and to cancel noise simultaneously. This can be interpreted as a trade-off between underfitting and overfitting. If the algorithm treats the noise as components of the signals, identifying noise would lead to overfitting, whereas, forgetting higher frequency components would cause underfitting. Furthermore, the

Table 1

Algorithms	Overall RMS Error/Hs (%)	Maximum 5-s RMS Error/Hs (%)	Training Intervals (s)
a. Sea state 1: Hs = 1.7 m, Tp = 8.7s			
Approximate Prony method based on ESPRIT	17.36	59.57	~6Tp = 52s
LS-SVM regression	13.16	32.33	AR model ~2Tp = 17s Training~60Tp = 522s
b. Sea state 2: Hs = 4.5m, Tp = 11.8s			
Approximate Prony method based on ESPRIT	14.74	36.63	~6Tp = 71s
LS-SVM regression	12.74	32	AR model ~2Tp = 24s Training~60Tp = 708s

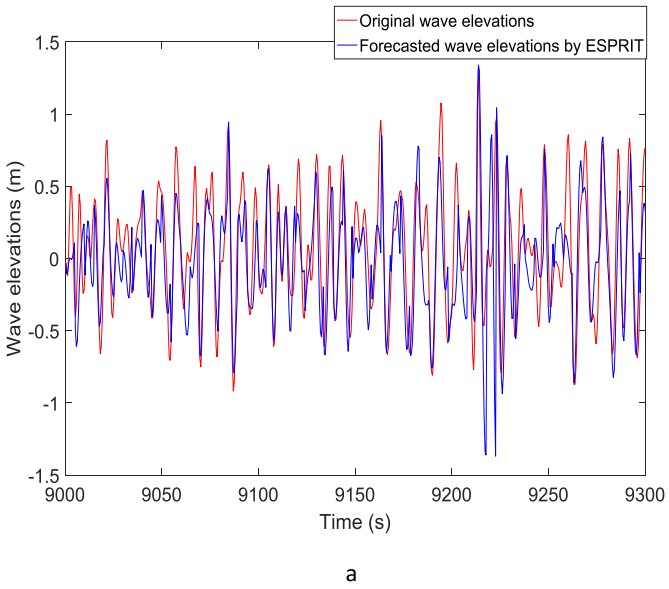

Fig. 1. a. Sea state 1: Approximate Prony method based on ESPRIT, RMS error = 18.47% Hs. b. Sea state 1: LS-SVM regression method, RMS error = 12.8% Hs.

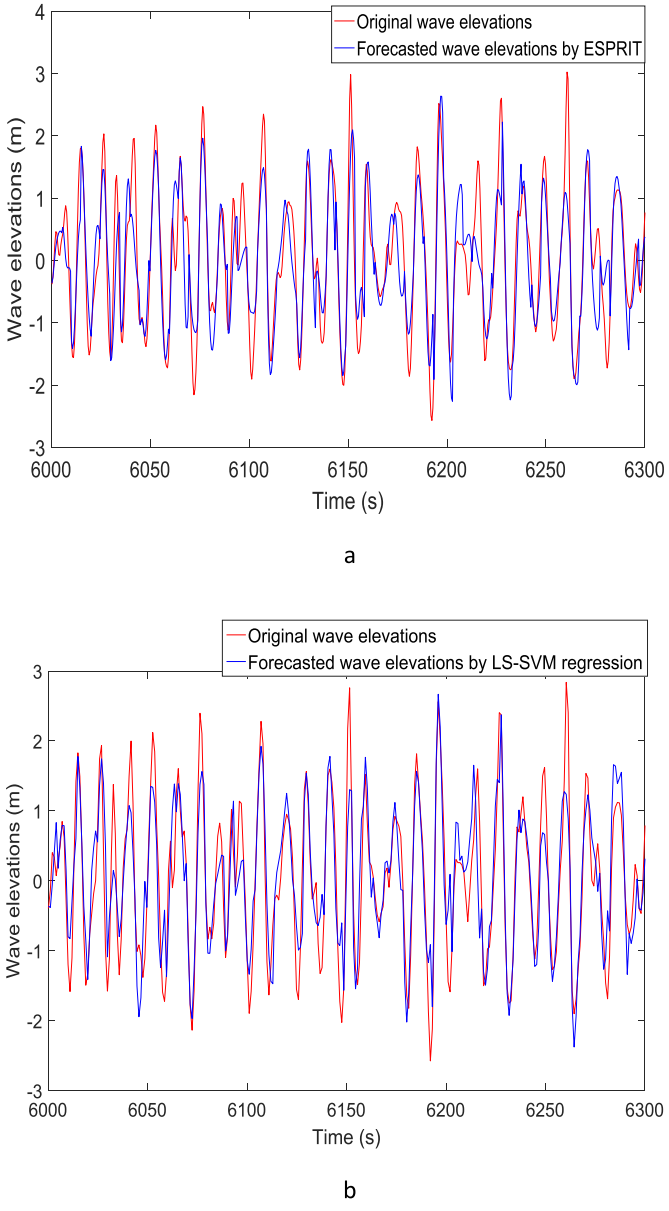

Fig. 2. a. Sea state 2: Approximate Prony method based on ESPRIT, RMS error = 12.73% Hs. b. Sea state 2: LS-SVM regression method, RMS error = 12% Hs.

real-time measured wave elevations or wave excitation forces are actually non-stationary signals. The frequency components that a finite length of wave elevation and wave force records contain are changing over time, so as is the signal to noise ratio.

From the results shown in Table 1 and Figure (1) and (2), the LS-SVM regression method has an overall better performance, for both the overall RMS error and worst-case RMS error, than the approximate Prony method based on ESPRIT. Moreover, the LS-SVM regression methods performs significantly better for the milder sea state (sea state 1). Fig. 3 is a comparison of the normalized wave spectrum of the two sea states. From the spectra, sea state 1 contains relatively more higher frequency components which makes it

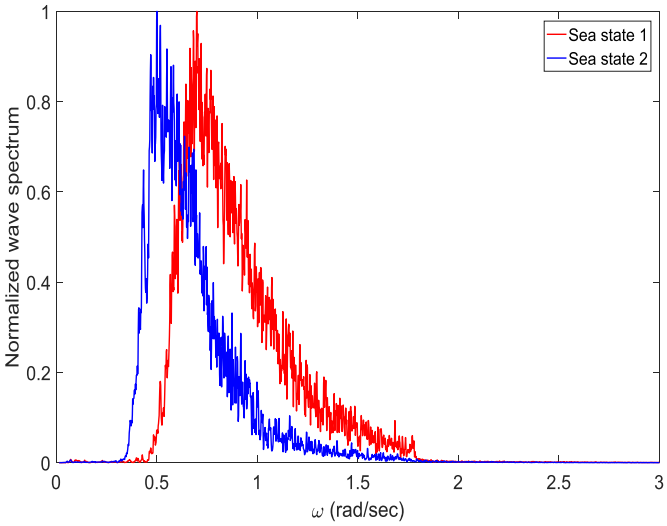

Fig. 3. Comparison of the normalized wave spectrum of the two sea states.

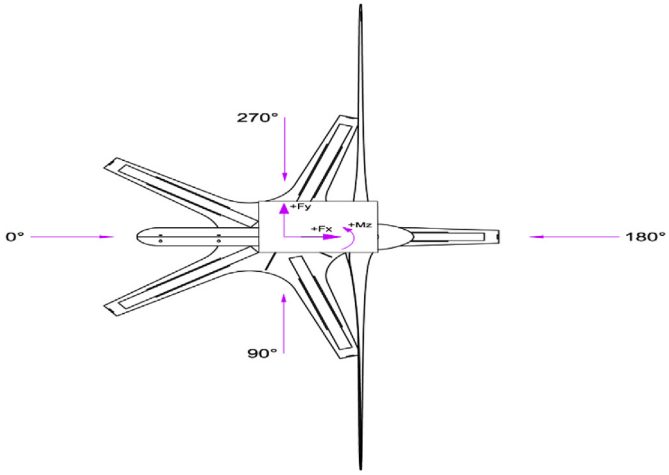

Fig. 4. A sketch of the coordinate system.

more difficult to forecast. LS-SVM regression method inherently prohibits over-fitting the signal and thus is more capable of distinguishing high frequency components from noise without causing too much overfitting, while the approximate Prony method based on ESPRIT performs better for signals with relatively lower frequency components and clean signals. In terms of the computational cost, the approximate Prony method needs fewer training samples than the LS-SVM regression leading to less computational time.

5. Simulation results of the optimal control for load reduction

A TLP supported floating wind turbine system is used to verify the optimal control algorithm. A more detailed introduction of the prototype can be found in the following references [19]; [20]. A sketch of the coordinate system associated with the floating wind turbine is shown in Fig. 4. The open-loop system dynamics is linearized around an operation point and the corresponding state space model of the wind turbine is generated using FAST (Fatigue, Aerodynamics, Structures, and Turbulence) code, which is a comprehensive aero-hydro-servo-elastic simulator for wind turbines [23]. A set of fully nonlinear FAST simulation cases with baseline controller were used for validation purposes.

5.1. Validation of the linear state space model

As described in (25), the wave excitation force is considered an external disturbance in this study. For operational conditions above rated wind speed, the control variable of the system is the blade pitch angle [22]. Using FAST, the open-loop system dynamics under calm water condition is linearized around an operation point above the rated wind speed:

$$\begin{cases} \Delta\dot{x} = A\Delta x + B\Delta\beta + B_d\Delta v \\ \Delta y = C\Delta x + D\Delta\beta + D_d\Delta v \end{cases} \tag{35}$$

where, Δx is the states deviating from steady values under the operation condition. In this study, Δx has totally 23 states describing the kinematic and structural characteristics of the floating wind turbine system. Δy is the output variables deviating from the corresponding steady values, in this study, Δy includes two tower base bending moments (side-side and fore-aft). $\Delta\beta$ is the blade pitch angle apart from the operation point. Δv is the incoming wind speed apart from the operation point. A, B, B_d, C, D, D_d are the corresponding state space matrices representing aero-elastic behavior of the 6 MW offshore wind turbine.

Since this study aims to apply an optimal control for reducing structural loads excited by wave excitation forces, the incoming wind is assumed to be known. In practice, the optimal control would be overlaid with the baseline rotor speed regulator, thus the linear model needs to be modified by adding a PI controller into the loop. The design of this baseline controller has taken the instability issue due to "negative damping" into consideration and a more detailed investigation is beyond the scope of this paper. Detailed information of the baseline controller can be found in Ref. [21].

The baseline PI controller regulating the rotor speed is added to (35) to form a revised linear model, with gains k_p and k_i. Then, the linear model is modified to:

$$\begin{cases} \Delta\dot{x} = A\Delta x + B\beta_{PI} + B_d\Delta v \\ \Delta y = C\Delta x + D\beta_{PI} + D_d\Delta v \end{cases} \tag{36}$$

where,

$$\beta_{PI}(t) = k_p e(t) + k_i \int_0^t e(\tau)d\tau \tag{37}$$

$$e(t) = x_{22}(t) - r = \Delta x_{22}(t) \tag{38}$$

where, $x_{22}(t)$ is the actual rotor speed. r is the reference value. $\Delta x_{22}(t)$ is the 22nd state of Δx in (36).

The PI controller (37)–(38) can be expressed in state space form by introducing an additional state:

$$\begin{cases} \dot{z} = e = \Delta x_{22} \\ \beta_{PI} = k_i z + k_p e = k_i z + k_p \Delta x_{22} \end{cases} \tag{39}$$

Plugging (39) into (36), the modified linear model becomes:

$$\begin{bmatrix} \Delta\dot{x} \\ \dot{z} \end{bmatrix} = \begin{bmatrix} A + BK_p & k_i B \\ [0,0,\ldots,1,0] & 0 \end{bmatrix} \begin{bmatrix} \Delta x \\ z \end{bmatrix} + \begin{bmatrix} B_d \\ 0 \end{bmatrix} \Delta v$$
$$\Delta y = \begin{bmatrix} C + DK_p & k_i D \end{bmatrix} \begin{bmatrix} \Delta x \\ z \end{bmatrix} + D_d \Delta v \tag{40}$$

where, $K_p = [0,0,\ldots,k_p,0]$.

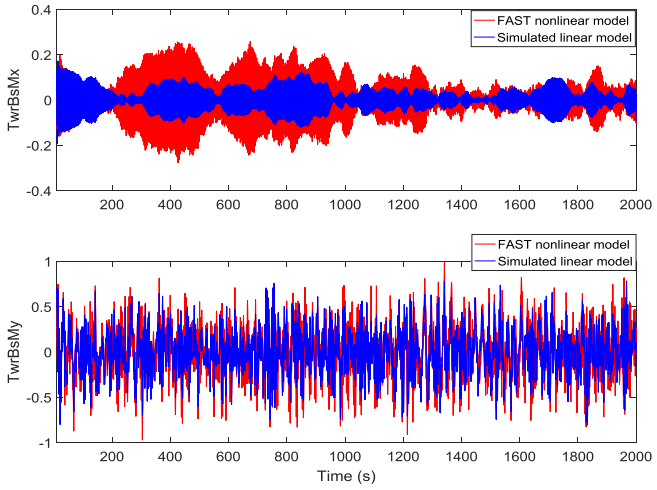

(a) Tower bending moments in time domain

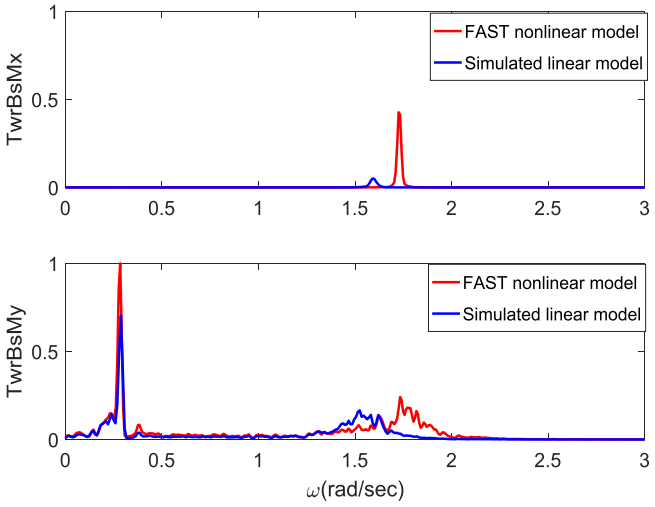

(b) Tower bending moments in frequency domain

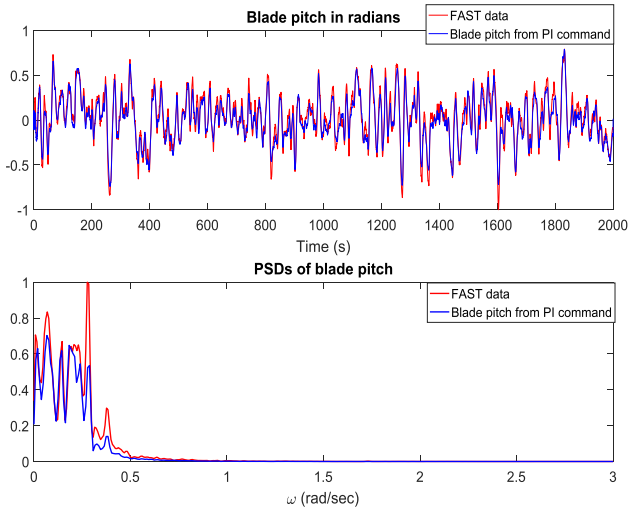

(c) Blade pitch angle

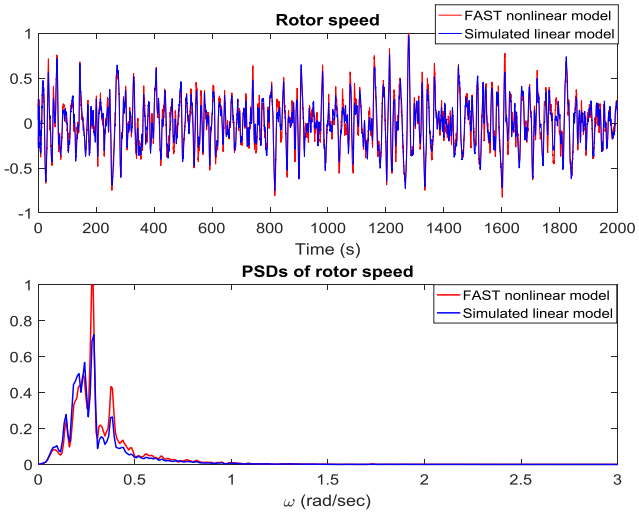

(d) Rotor speed

Fig. 5. Comparison of the linearized model and FAST nonlinear simulation under calm water.

To validate the linear model, Eq. (40) is solved numerically in the time domain. The model is validated under the calm water condition. The same wind velocity is input to the linear model as in FAST nonlinear simulations. The mean wind velocity is 16 m/s and the turbulence intensity is about 0.0564, which is above rated-speed and temporally coherent. Under the calm water condition, there is no incident wave excitation force and the effects of wave radiation force have already been included in the state space model. Therefore, under such wind-only conditions, model (40) should ideally capture all the system dynamics. The comparisons of output variables (fore-aft tower base bending moment TwrBsMy and side-side tower base bending moment TwrBsMx), control variable (blade pitch angle) and concerned states (rotor speed) between the linear model and the FAST nonlinear simulations are shown in Fig. 5.

All the concerned physical quantities in this section are normalized to $[-1, 1]$ and the non-dimensional results should not affect the discussions and conclusions drawn from this study.

From Fig. 5, it can be seen that the linear model (40) captures

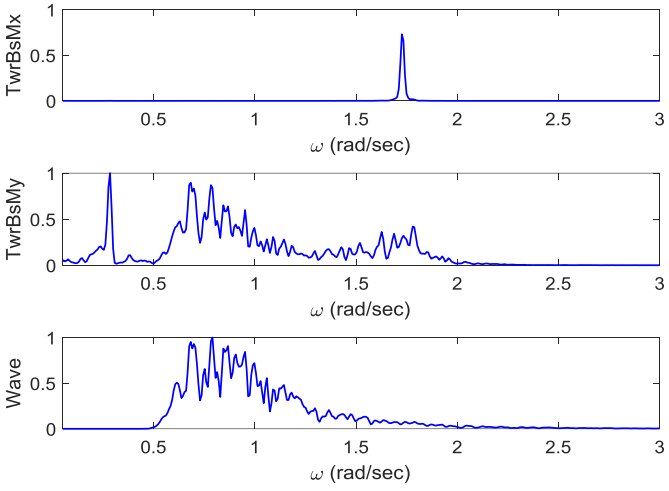

Fig. 6. Power spectrum of irregular wave (Hs = 2.75 m, Tp = 8s) and corresponding tower bending moments simulated by FAST.

Table 2
Wind and wave conditions for the five tested cases.

Case No.	Wind	Wave		
		Hs	Tp	Heading
Case 1	Coherent turbulent wind, mean speed 16 m/s, turbulence intensity 0.0564	2.75	8	Zero degree
Case 2	Coherent turbulent wind, mean speed 16 m/s, turbulence intensity 0.0564	3.5	11	Zero degree
Case 3	Coherent turbulent wind, mean speed 16 m/s, turbulence intensity 0.0564	2.75	8	Spread sea, main wave heading is zero degree

most of the system dynamics affecting the fore-aft tower base moment under the calm water condition, while it has a significant gap for the side-side tower base moment. Fig. 6 shows a frequency domain result of the tower bending moments under the same wind condition but also with an irregular wave sea state (Hs = 2.75 m, Tp = 8s) by nonlinear FAST simulations. From Fig. 6, it can be shown that the side-side tower base bending moment (TwrBsMx) is mostly dominated by the first tower bending mode (around 1.5–2 rad/sec). In the other hand, the fore-aft bending moment (TwrBsMy) has multiple peaks corresponding to platform surge resonance frequency (around 0.25 rad/sec), wave excitation frequencies (around 0.5–1.5 rad/sec) and the first tower bending mode (around 1.5–2 rad/sec). Clearly, wave excited loads have a major impact on the fore-aft bending moment (TwrBsMy). Since the major objective of this study is to reduce the wave excited fore-aft tower base moment, the linear model (40) is considered reasonable enough to proceed with the implementation of optimal control.

5.2. Implementation of the finite-horizon LQR controller with predictor

The actual system dynamics under the irregular wave condition is:

$$\begin{bmatrix}\Delta\dot{x}\\ \dot{z}\end{bmatrix} = \begin{bmatrix}A+BK_p & k_iB\\ [0,0,\ldots,1,0] & 0\end{bmatrix}\begin{bmatrix}\Delta x\\ z\end{bmatrix} + \begin{bmatrix}B_d\\ 0\end{bmatrix}\Delta v + f_e$$
$$\Delta y = \begin{bmatrix}C+DK_p & k_iD\end{bmatrix}\begin{bmatrix}\Delta x\\ z\end{bmatrix} + D_d\Delta v \tag{41}$$

where, f_e is the wave excitation force vector.

Evaluate f_e as follows assuming knowledge of the system states:

$$f_e = \begin{bmatrix}\Delta\dot{x}\\ \dot{z}\end{bmatrix} - \begin{bmatrix}A+BK_p & k_iB\\ [0,0,\ldots,1,0] & 0\end{bmatrix}\begin{bmatrix}\Delta x\\ z\end{bmatrix} - \begin{bmatrix}B_d\\ 0\end{bmatrix}\Delta v \tag{42}$$

where, $\Delta x, z, \Delta v$ are real-time measurements of the system states and wind speeds when evaluating the force vector f_e.

If the linear model matches the system dynamics exactly, f_e would be the incident wave excitation force. However, from results shown in Fig. 5, there is a large gap for the side-side tower bending moment. This indicates that f_e evaluated from (42) would include components introduced by this modeling error. We consider f_e derived from Eq. (42) as an equivalent forcing vector that can be measured online in terms of the system states and predict it using the approximate Prony method based ESPRIT or LS-SVM regression.

With the knowledge of predicted equivalent wave disturbance terms f_e, the finite-horizon LQR problem (27)–(32) can be solved. And the system dynamics with the optimal control effort u_{opt} can be derived in time domain (33).

5.3. Simulation results of the finite-horizon LQR with prediction of equivalent wave force

To validate the finite-horizon LQR with the prediction of equivalent wave force vector, three different scenarios are tested and compared with the baseline controller. The FAST simulations with baseline controller are 2000-s long. The finite-horizon LQR problem subject to the modified linear state space model (41) is solved in the time domain using FAST simulation data as initializations. The LQR controller is turned on at t = 200s.

The time step of the numerical solver for the optimization problem and system dynamics are set to be 0.025 s based on convergence tests. The optimal controller update rate is 1 s and the optimization horizon T in Eq. (26) is 1 s, which is also the forecast horizon of the equivalent forcing vector f_e. The average value of blade pitch angle solved from (27) is applied until the next controller update.

The controller with the predictor is tested under three different scenarios. The mean value of wind velocity is 16 m/s as the linearization point. In addition, a coherent turbulence model is used to generate the actual wind time series. Two unidirectional wave conditions with different significant wave heights and typical wave periods are tested in the simulations, which both have zero degree wave headings. Furthermore, the controller and the predictor are also tested under spread sea conditions. The main wave heading is zero degrees and a Cosine-2s spreading model is used. The combination of wind and wave conditions for the three tested cases are listed in Table 2.

The performance of the overlaid optimal controller is measured by the percentage of changes for variables of concern:

$$\frac{Var\left(Y_{optimal}\right) - Var(Y_{baseline})}{Var(Y_{baseline})}\% \tag{43}$$

where, Y could be the fore-aft tower bending moment TwrBsMy, side-side tower bending moment TwrBsMx and rotor speed. $Var(\bullet)$ denotes the variance of the concerning variables. The variance of tower bending moments is treated as an indirect measure of fatigue loading.

Taking account of the actuator limits, the maximum blade pitch rate is normally up to 7°/second. The trade-off between the performance and control efforts are adjusted through the penalty matrix Q and R in (26). The weighting matrices S and G in (26) are set to be zero.

Table 3
Performance of the finite-horizon LQR with predictor.

Case No.	TwrBsMx (side-side) (%)	TwrBsMy (fore-aft) (%)	Rotor speed variation (%)	Maximum blade pitch rate (deg/sec)
Case 1	+19.87	−69.86	+28.94	6.8
Case 2	+17.65	−55.74	+14.32	6.84
Case 3	−0.58	−67.34	+17.80	6.76

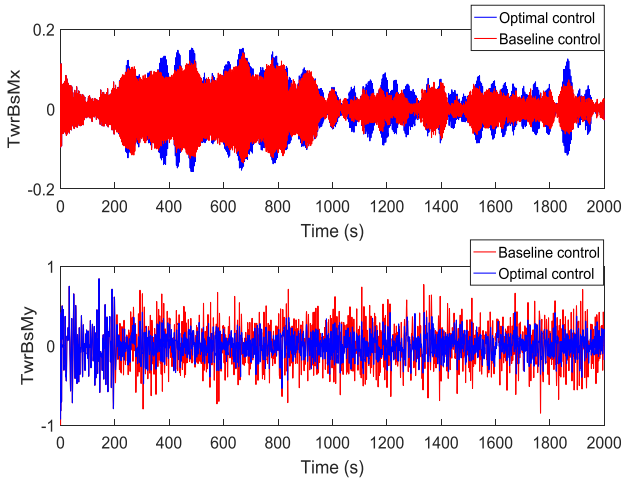

(a) Tower bending moments in time domain

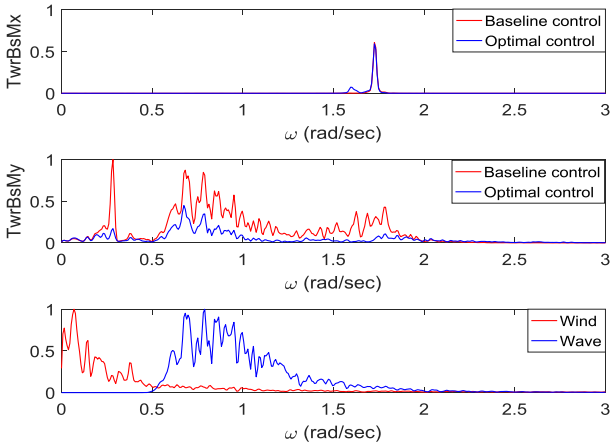

(b) Tower bending moments and input wind wave conditions in frequency domain

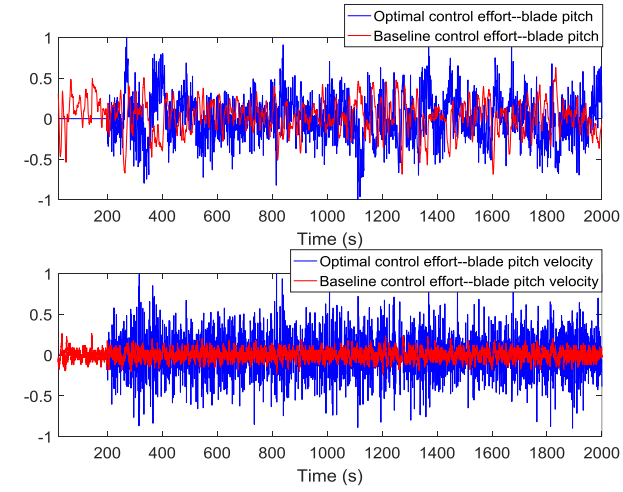

(c) Control efforts: blade pitch angle and blade pitch velocity

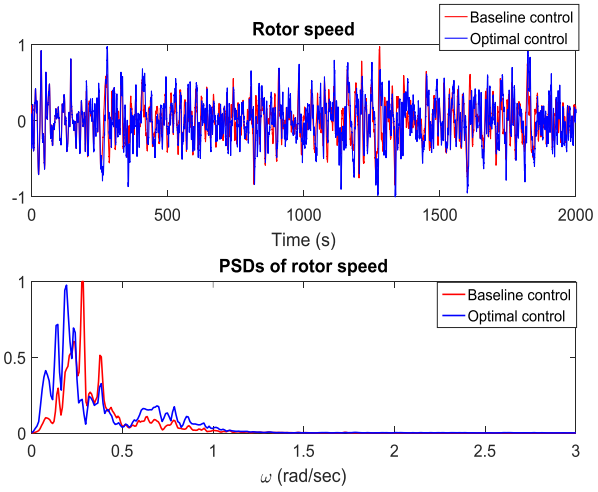

(d) Rotor speed

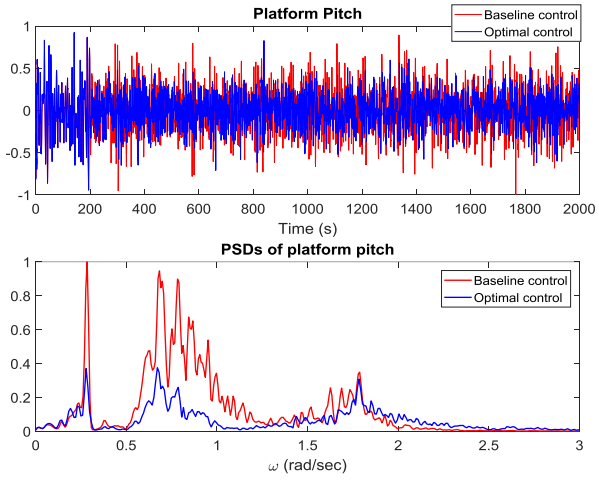

(e) Platform pitch motion

Fig. 7. Case 1: Comparison of the optimal control and baseline controller.

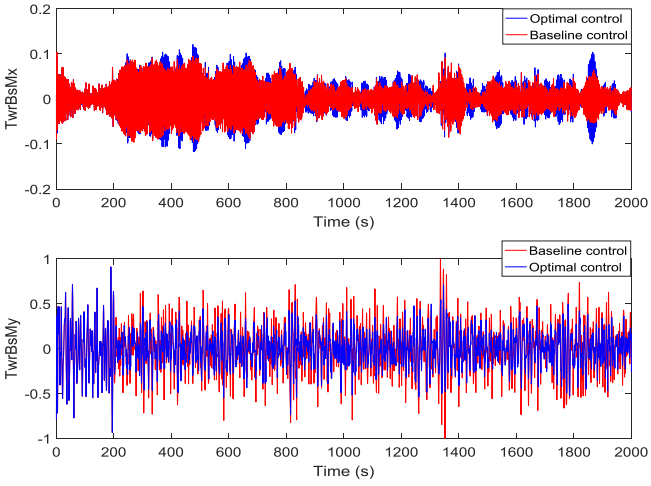

(a) Tower bending moments in time domain

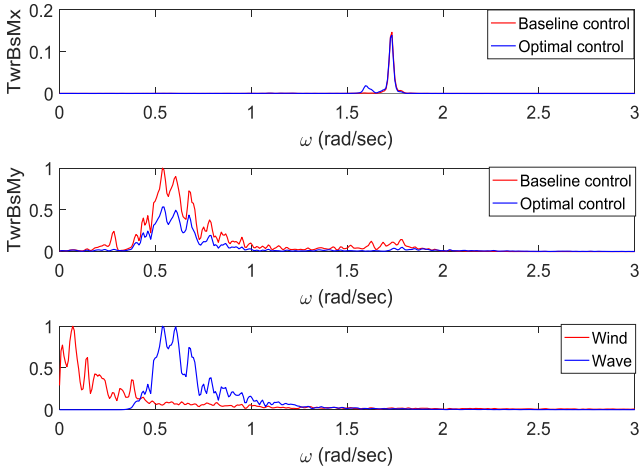

(b) Tower bending moments and input wind wave conditions in frequency domain

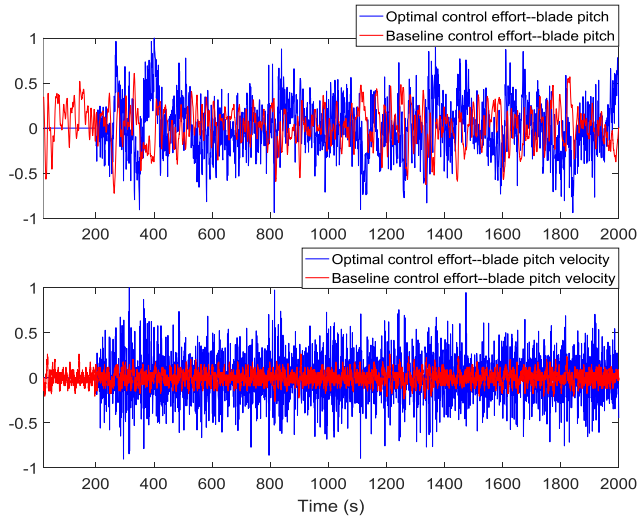

(c) Control efforts: blade pitch angle and blade pitch velocity

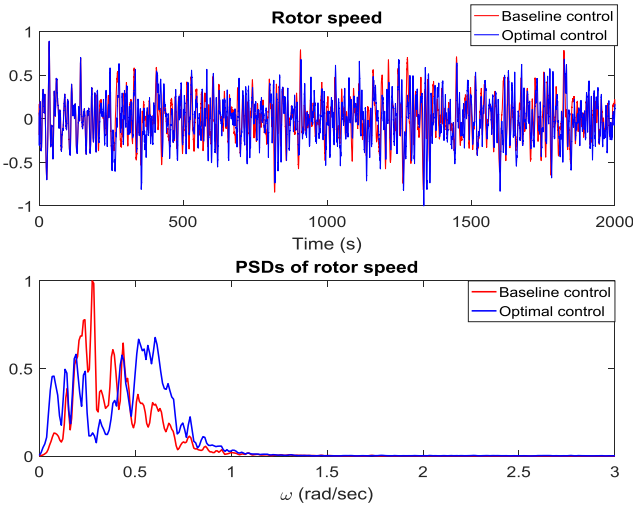

(d) Rotor speed

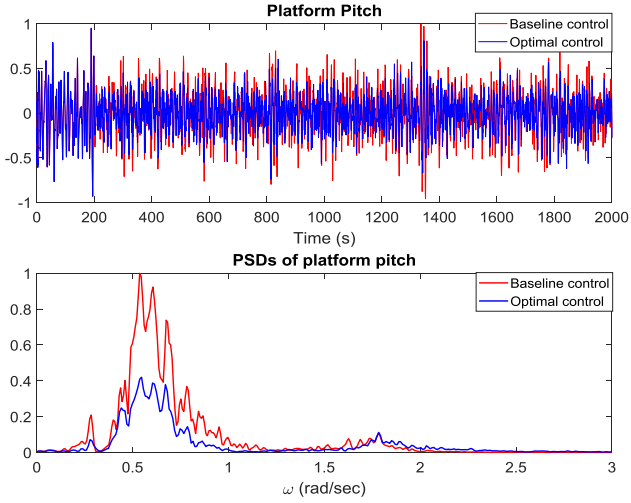

(e) Platform pitch motion

Fig. 8. Case 2: Comparison of the optimal control and baseline controller.

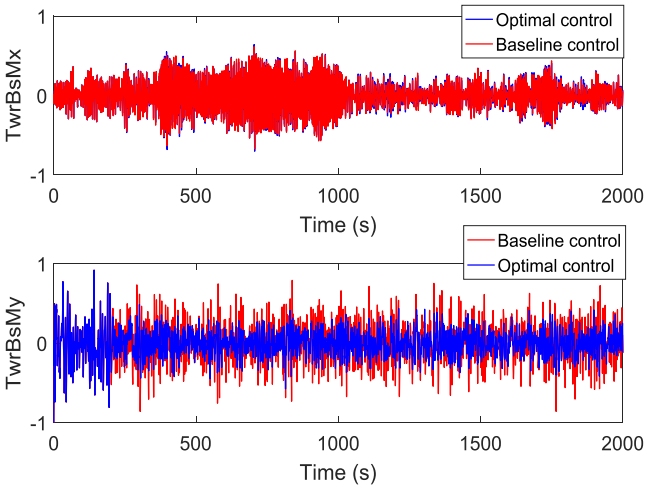

(a) Tower bending moments in time domain

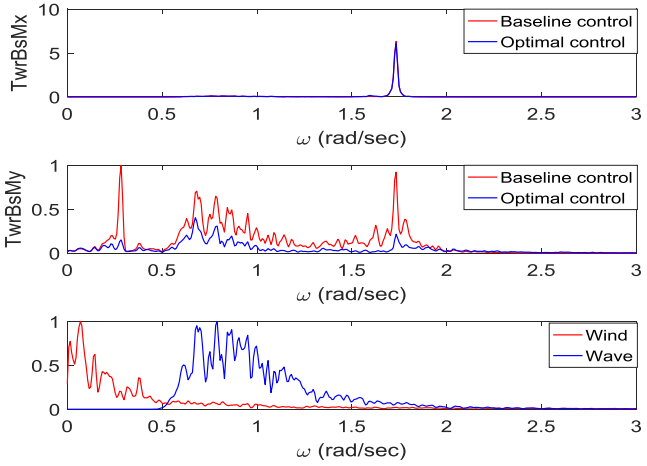

(b) Tower bending moments and input wind wave conditions in frequency domain

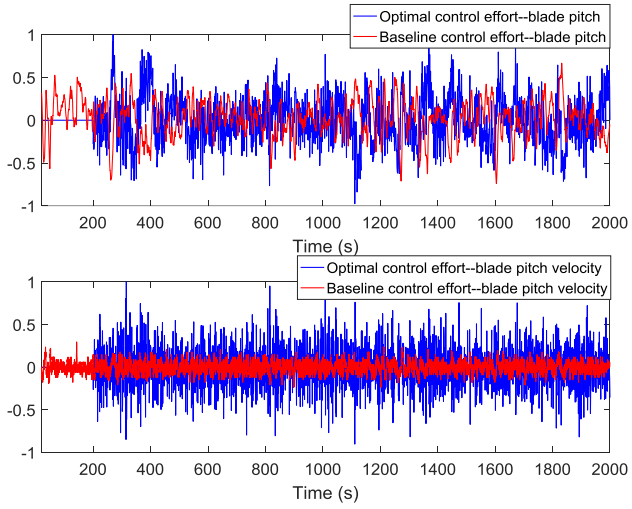

(c) Control efforts: blade pitch angle and blade pitch velocity

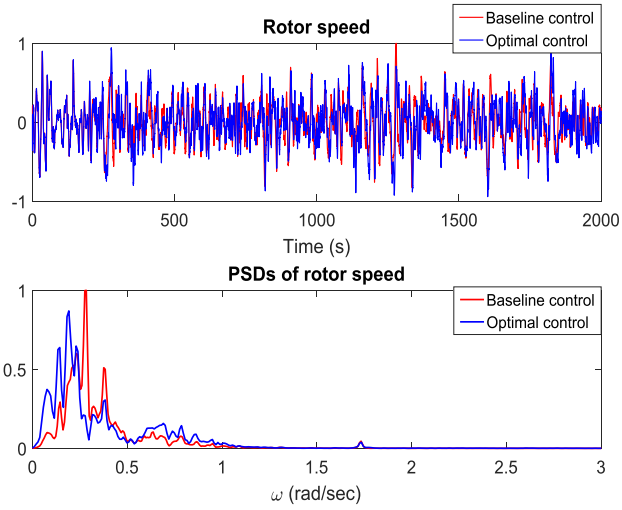

(d) Rotor speed

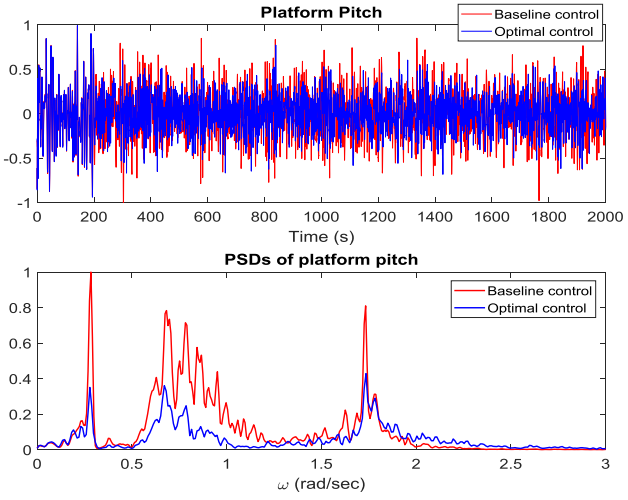

(e) Platform pitch motion

Fig. 9. Case 3: Comparison of the optimal control and baseline controller.

The performance of the finite-horizon LQR controller with the prediction of the equivalent forcing vector is summarized in Table 3 and Figures (7)–(9). From the results, the finite-horizon LQR controller with prediction of the equivalent wave force vector significantly reduces the fore-aft tower base bending moment. Meanwhile, the side-side tower bending moment and rotor speed variation are slightly increased as a cost, which is acceptable since the side-side tower bending moment is far lower than that in the fore-aft direction thus not leading to increased structural requirements. In addition, depending on different concerns of structural safety or power stabilization, the effects of the optimal controller on different quantities can be adjusted via the penalty matrix in the optimization process.

As for the optimal controller itself, the performance is influenced by the optimization horizon, accuracy of the predictor, tradeoff of the elements in LQR weighting matrices, etc. Furthermore, the input wind and wave conditions and accuracy of the linearization process would also have significant effects on the overall performance for the load reduction. From the results, the proposed LQR controller as well as the predictor is robust performing consistently under different wave conditions and is capable of tolerating non-negligible modeling residues in the linearization process.

6. Conclusion and discussion

In this study, successful wave elevation and exciting force forecast algorithms have been developed for use in optimal control on load reduction. Two forecast algorithms, the approximate Prony method based on ESPRIT and the LS-SVM regression method, are developed and validated using real-time measurements.

On the basis of the ability to forecast the wave force over a finite horizon into the future, a deterministic finite-horizon LQR controller is designed to reduce the fore-aft tower base bending moment, especially the components excited by the wave force. The performance of the optimal control is effective and robust for the aimed load reduction comparing to the baseline speed regulator.

The general predictability of a sea state is a difficult question to answer in principle since real sea states are nonstationary and multi-directional. Therefore, we rely on the performance of the forecast algorithms in our paper and do not address the more fundamental question of how forecastable real seastate elevations are. The error in the forecasts generated by the algorithms consist of three components a) algorithm bias b) algorithm variance c) noise. Alternative algorithms introduce different bias vs variance tradeoffs, which is a topic that we do not address in this paper as well. Ambient noise is unforecastable by any algorithm. The relative magnitude of these three sources of error is only possible after a systematic study among alternative algorithms and parameters within each algorithm. This topic is beyond the scope of the present paper and will be addressed in the future work.

Therefore, considering the forecast algorithm itself, the performance would degenerate significantly as the forecast horizon gets larger. The tradeoff between the forecast accuracy and required forecast horizon should be balanced depending on specific problems and objectives. In the context of this paper, the forecast accuracy of the wave elevations up to a 5-s horizon is considered by the ESPRIT and SVM algorithm and found to be good. Meanwhile, this time scale is also considered as sufficient for controller design purposes.

In future work, more detailed sensitivity studies will be conducted in terms of the effects of the optimization horizon, controller update rate and predictor accuracy. Furthermore, on-line linearization and optimization techniques would be considered for better real-time implementations. The computational effort necessary to generate the forecasted signals needs to be addressed so that the on-line implementation can be achieved efficiently for sequential controller updates.

The control algorithm developed in this paper for a stiff TLP floating wind turbine may be also implemented with minor modifications for “softer” floating wind turbine concepts like Spars and Semisubmersibles. For example, the effectiveness of blade-pitch controllers has been already demonstrated for the Hywind concept for the mitigation of responses at frequencies well below the peak of the wave spectrum. Meanwhile, this approach is also promising for different control targets combined with the ability to forecast wind speed.

Acknowledgements

This research is based upon work supported by the Department of Energy under Award Number #DE-EE0005494. This financial support is gratefully acknowledged.

References

[1] A. Korber, R. King, Model predictive control for wind turbines, in: Proceedings of EWEC, 2010, April.
[2] J. Laks, L.Y. Pao, A. Wright, N. Kelley, B. Jonkman, Blade pitch control with preview wind measurements, in: Proc. 48th AIAA Aerospace Sciences Meeting, Orlando, FL, 2010, January. AIAA-2010-251.
[3] S. Raach, D. Schlipf, F. Sandner, D. Matha, P.W. Cheng, Nonlinear model predictive control of floating wind turbines with individual pitch control, in: 2014 American Control Conference, IEEE, 2014, June, pp. 4434–4439.
[4] E.N. Wayman, P.D. Sclavounos, S. Butterfield, J. Jonkman, W. Musial, Coupled dynamic modeling of floating wind turbine systems, in: Offshore Technology Conference. Offshore Technology Conference, 2006, January.
[5] T.J. Larsen, T.D. Hanson, A method to avoid negative damped low frequent tower vibrations for a floating, pitch controlled wind turbine, in: Journal of Physics: Conference Series, IOP Publishing, 2007, p. 012073 vol. **75**, No. 1.
[6] J. Hals, J. Falnes, T. Moan, Constrained optimal control of a heaving buoy wave-energy converter, J. Offshore Mech. Arctic Eng. 133 (1) (2011), 011401.
[7] F. Fusco, J.V. Ringwood, Short-term wave forecasting for real-time control of wave energy converters, IEEE Transactions on Sustainable Energy 1 (2) (2010) 99–106.
[8] C.C.B. Casanovas, Advanced Controls for Floating Wind Turbines, Thesis: S.M., Massachusetts Institute of Technology, 2014.
[9] D. Potts, M. Tasche, Parameter estimation for exponential sums by approximate Prony method, Signal Process. 90 (5) (2010) 1631–1642.
[10] V. Pereyra, G. & Scherer (Eds.), Exponential Data Fitting and its Applications, Bentham Science Publishers, 2010.
[11] T.B. Trafalis, H. Ince, Support vector machine for regression and applications to financial forecasting, in: IJCNN, vol. 6, 2000, June, pp. 348–353.
[12] J. Zhou, J. Shi, G. Li, Fine tuning support vector machines for short-term wind speed forecasting, Energy Convers. Manag. 52 (4) (2011) 1990–1998.
[13] S. Salcedo-Sanz, E.G. Ortiz-Garcı, Á.M. Pérez-Bellido, A. Portilla-Figueras, L. Prieto, Short term wind speed prediction based on evolutionary support vector regression algorithms, Expert Syst. Appl. 38 (4) (2011) 4052–4057.
[14] J.A. Suykens, J. Vandewalle, Least squares support vector machine classifiers, Neural Process. Lett. 9 (3) (1999) 293–300.
[15] J. Yong, X.Y. Zhou, Stochastic Controls: Hamiltonian Systems and HJB Equations, vol. 43, Springer Science & Business Media, 1999.
[16] P. Naaijen, E. Blondel-Couprie, Reconstruction and prediction of short-crested seas based on the application of a 3D-FFT on synthetic waves: Part 1—Reconstruction, in: ASME 2012 31st International Conference on Ocean, Offshore and Arctic Engineering, American Society of Mechanical Engineers, 2012, July, pp. 43–53.
[17] C.H. Lee, J.N. Newman, WAMIT User Manual, WAMIT, Inc, 2006.
[18] K. Duan, S.S. Keerthi, A.N. Poo, Evaluation of simple performance measures for tuning SVM hyperparameters, Neurocomputing 51 (2003) 41–59.
[19] L. Vita, G.K.V. Ramachandran, A. Krieger, M.I. Kvittem, D. Merino, J. Cross-Whiter, B.B. Ackers, Comparison of numerical models and verification against experimental data, using PelaStar TLP concept, in: ASME 2015 34th International Conference on Ocean, Offshore and Arctic Engineering, American Society of Mechanical Engineers, 2015, May (pp. V009T09A047–V009T09A047).
[20] Rodriguez A. Tsouroukdissian, M. Lackner, J. Cross-Whiter, S.M. Park, P. Pourazarm, W. La Cava, S. Lee, Smart Novel Semi-active Tuned Mass Damper for Fixed-bottom and Floating Offshore Wind (No. DOE-alstom-0005494), Alstom Renewable US LLC (GE Subsidiary), aka-Alsom Power Inc, 2016.
[21] P.A. Fleming, I. Pineda, M. Rossetti, A.D. Wright, D. Arora, Evaluating methods for control of an offshore floating turbine, in: ASME 2014 33rd International

Conference on Ocean, Offshore and Arctic Engineering, American Society of Mechanical Engineers, 2014, June (pp. V09BT09A019–V09BT09A019).
[22] J. Jonkman, S. Butterfield, W. Musial, G. Scott, Definition of a 5-MW Reference Wind Turbine for Offshore System Development (No. NREL/TP-500-38060), National Renewable Energy Laboratory (NREL), Golden, CO, 2009.
[23] J.M. Jonkman, M.L. Buhl Jr., FAST User's Guide-updated August 2005 (No. NREL/TP-500–38230), National Renewable Energy Laboratory (NREL), Golden, CO, 2005.